High-Temperature-Induced Phase Transitions in Honeycomb Layered Oxides $A_2Ni_2TeO_6$ (A = Na, K)

Josef Rizell[a], Godwill Mbiti Kanyolo[d], Titus Masese[b,c], Yasmine Sassa[a] and Zhen-Dong Huang[e]

[a] Department of Physics, Chalmers University of Technology, SE–412 96, Göteborg, SWEDEN.
[b] Research Institute of Electrochemical Energy, National Institute of Advanced Industrial Science and Technology (AIST), 1–8–31 Midorigaoka, Ikeda, Osaka 563–8577, JAPAN.
[c] AIST–Kyoto University Chemical Energy Materials Open Innovation Laboratory (ChEM-OIL), Sakyo–ku, Kyoto 606–8501, JAPAN. Email: titus.masese@aist.go.jp
[d] Department of Engineering Science, The University of Electro-Communications, 1–5–1 Chofugaoka, Chofu, Tokyo 182–8585, JAPAN.
[e] Key Laboratory for Organic Electronics and Information Displays and Institute of Advanced Materials (IAM), Nanjing University of Posts and Telecommunications (NUPT), Nanjing, 210023, CHINA.

Abstract

Phase transitions have been surmised as underlying factors behind the exceptional electrochemical, ionic and magnetic functionalities that have catapulted honeycomb layered oxides as superb functional materials. As such, in this study (*short communication*), we explore temperature elevation as an avenue for inducing phase transitions in honeycomb layered oxides adopting the composition $A_2M_2TeO_6$ (*A* = Li, Na, K; *M* = (transition) metal). X-ray diffraction analyses indicate structural changes occurring in $Na_2Ni_2TeO_6$ hexagonal lattice (centrosymmetric $P6_3/mcm$ → accentric $P6_3(22)$ space group) with increase in temperature, whilst in the potassium homologue ($K_2Ni_2TeO_6$), the phase transitions entail multiple changes in the lattice (from the initial hexagonal → monoclinic (pseudo-orthorhombic) lattice at intermediate temperatures) which reverts back to its initial hexagonal lattice with further increase in temperatures. This study opens an alternative channel for generating phase transition beside electrochemical alkali (re)insertion.

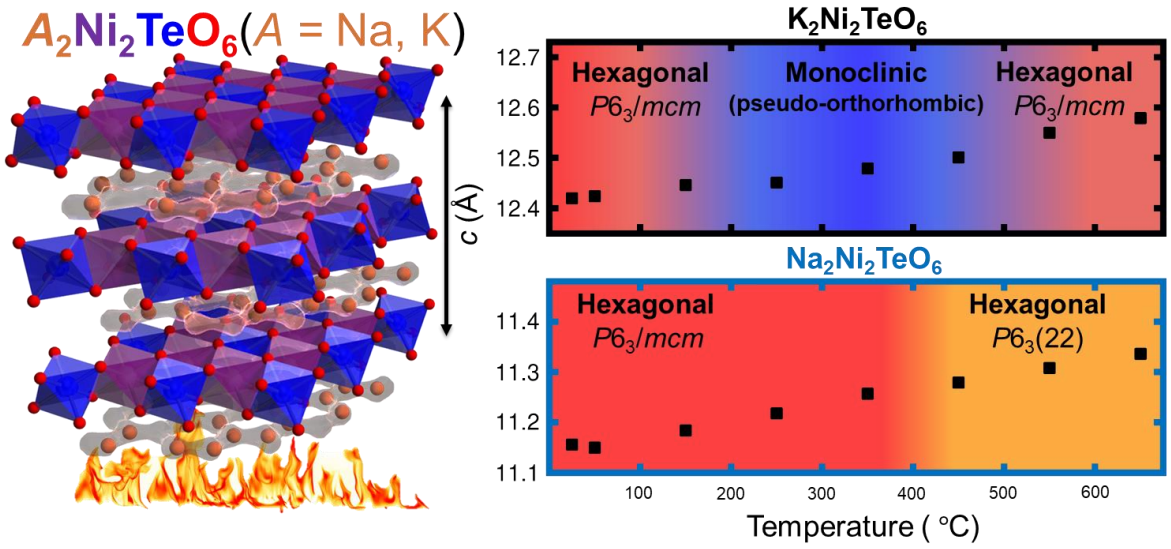

INTRODUCTION

Honeycomb layered oxides embodied by monovalent atoms such as Li, Na, K, Cu or Ag interposed between layers of transition metal oxides aligned in a honeycomb framework,[1] present a rich compositional space that harbours unparalleled set of capabilities such as fascinating magnetic interactions, agile ionic mobility, exotic phase transitions and exquisite electrochemical functionalities that draw immense interest in a wide range of applications in science and technology. [1–11] As such, extensive research efforts have been dedicated towards the development of these exemplar materials, particularly those adopting the chemical composition $A_2M_2TeO_6$ (A = Li, Na, K; M = transition or alkaline-earth metals), not only as high-voltage battery components[12–19] but also as a pedagogical platform for investigating unique magnetic phenomena. [2–11]

At elevated temperatures of around 300 °C, where high-temperature energy storage systems like sodium-sulphur (Na-S) batteries operate,[20] several honeycomb layered oxide materials have exhibited exemplary conductivities. $Na_2Ni_2TeO_6$ displays the highest ionic conductivity reaching a value of 10.1–10.8 S/m at 300 °C,[1,21] showing its potential as a superfast ionic conductor. Moreover, related honeycomb layered oxides such as $Na_2Zn_2TeO_6$ have been shown to be fast superionic conductors with applications as solid electrolytes for Na-ion batteries.[22–24] Superionic phase transitions attributed to structural changes in the crystal lattice symmetry primarily occur at elevated temperatures.[25,26] Therefore, it is crucial to investigate the structural changes intermittent in $Na_2Ni_2TeO_6$ and related honeycomb layered oxides.

In particular, $Na_2Ni_2TeO_6$ crystallises in a hexagonal lattice ($P6_3/mcm$ space group), as shown in **Figure 1a**. Na atoms coordinated with oxygen atoms reside between slabs of transition metals arranged in a honeycomb fashion. As shown in **Figure 1b** the honeycomb arrangement is characterised by clusters of one TeO_6 octahedra surrounded by six NiO_6 octahedra. Although a potassium analogue ($K_2Ni_2TeO_6$) has been reported to bear isostructural semblance to $Na_2Ni_2TeO_6$ **(Figure 1c)**, it constitutes a larger interlayered distance ascribed to the larger ionic radius of K^+ (1.38 Å)[27] in comparison to Na^+ (1.02 Å).[27]As a result, disparate phase transitions that result in distinctive stacking sequences can be anticipated when the two materials are subjected to high temperatures or electrochemical alkali-ion extraction. To validate this hypothesis, XRD measurements were performed on $Na_2Ni_2TeO_6$ and $K_2Ni_2TeO_6$ at high temperatures, revealing various phase transitions as detailed hereafter.

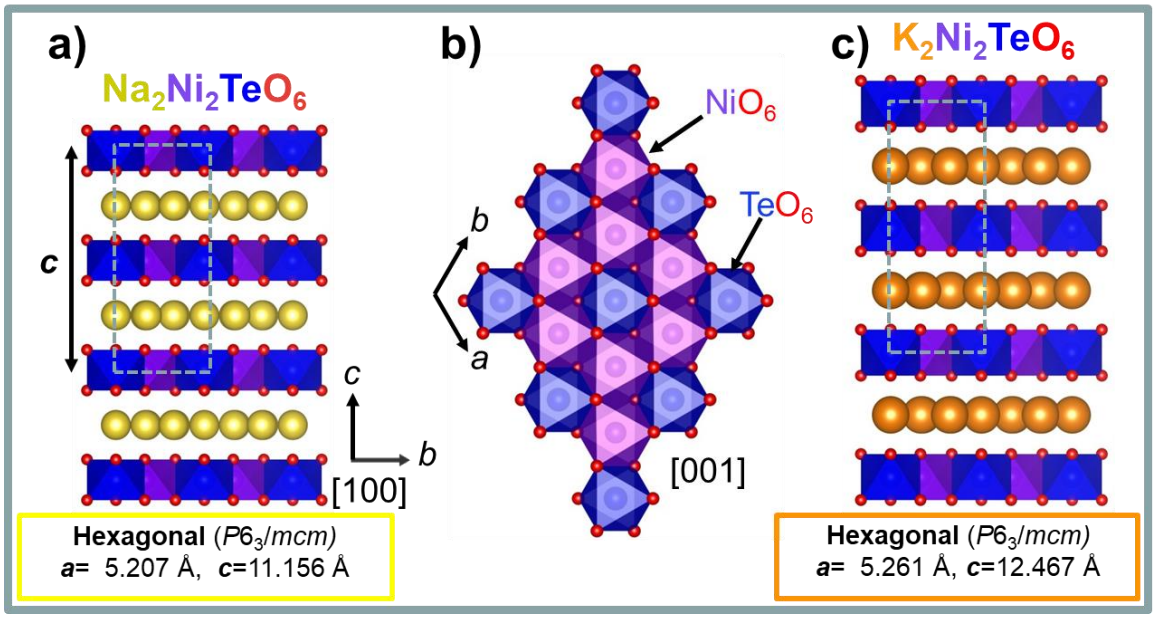

Figure 1. Crystal models of $Na_2Ni_2TeO_6$, the honeycomb slab and $K_2Ni_2TeO_6$. (a) The honeycomb layered structure of $Na_2Ni_2TeO_6$ with Na atoms sandwiched between slabs of NiO_6 and TeO_6 octahedra. **(b)** The honeycomb configuration of the transition metal slab with each atom of TeO_6 surrounded by six atoms of NiO_6. **(c)** Crystal structure of the isostructural $K_2Ni_2TeO_6$ illustrating the larger K atoms residing in the large interslab distance (*c*).The Shannon-Prewitt ion size difference between K^+ and Na^+ ions endows $K_2Ni_2TeO_6$ with a larger interslab spacing than $Na_2Ni_2TeO_6$. The unit cell for $A_2Ni_2TeO_6$ (*A* = Na, K) is denoted in dashed lines.

RESULTS & DISCUSSION

$A_2Ni_2TeO_6$ (*A* = Na, K) was synthesised using the conventional solid-state ceramics route, as specified in the **Supplementary Information** section. The crystallinity and the purity of the as-synthesised materials were confirmed using X-ray diffraction (XRD) analyses, indexing the materials univocally to the hexagonal lattice ($P6_3/mcm$ space group). Thermal stability analyses confirm that $A_2Ni_2TeO_6$ (*A* = Na, K) are stable to temperatures above 800 °C (**Supplementary Figure 1**), precluding phase changes relating to thermal decomposition within the temperature regimes assessed in this study. As the temperature increases, a phase transition is observed at 400 °C hallmarked by the emergence of new Bragg peaks and the disappearance of others, as shown the XRD

patterns for $Na_2Ni_2TeO_6$ (**Figure 2a** and **2b**). The emergence of new diffraction peaks such as (101) Bragg peak, which is forbidden in the $P6_3/mcm$ hexagonal space group but allowed in space groups such as $P6_322$, $P6_3$ and $P6_3/m$, prompted further profile fitting of the XRD pattern. Although both $P6_322$ and $P6_3$ space groups yield high reliability statistics, a more realistic structural model could be obtained when tentatively refined in the $P6_322$ space group model which is typically adopted by isostructural compositions such as $Na_2M_2TeO_6$ (M = Co, Zn, Cu, Mg).[21]

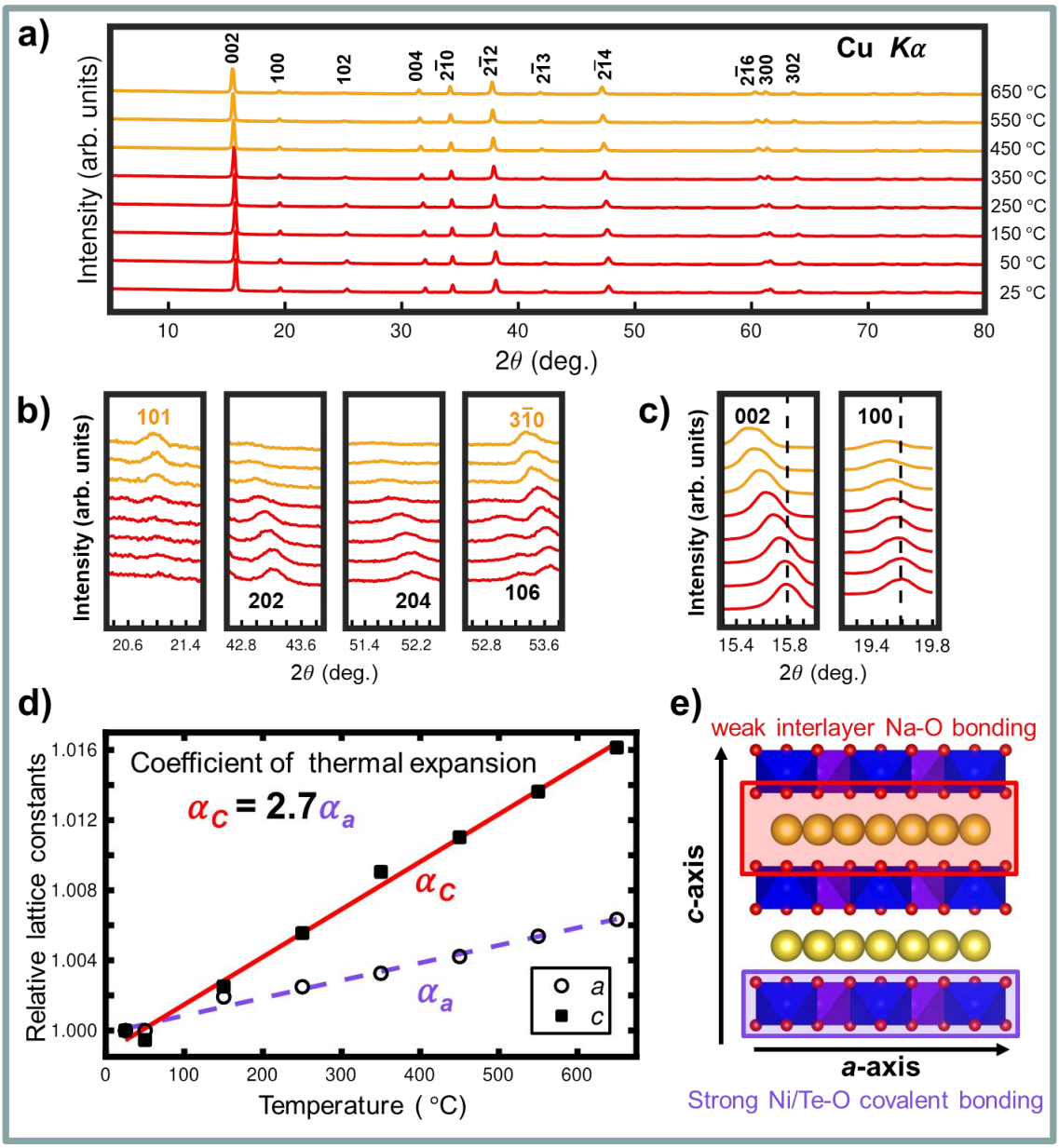

Figure 2. **High-temperature X-ray diffraction (XRD) measurements of $Na_2Ni_2TeO_6$.** **(a)** XRD patterns of $Na_2Ni_2TeO_6$ taken between 25 °C (298 K) and 650 °C (923 K).

Room-to-intermediate-temperature phase is highlighted in red, whereas the high-temperature phase is shown in orange, all indexable to hexagonal lattice space groups. **(b)** Emergence and disappearance of Bragg diffraction peaks, indicative of a phase transition entailing change in lattice symmetry. **(c)** Shift of (002) and (100) Bragg diffraction peaks to lower diffraction angles with increasing temperature indicating lattice expansion due to thermal perturbation. **(d)** Quantification of the lattice expansion with increase in temperature by plotting the *a* and *c* lattice constants against the temperature. The coefficient of thermal expansion along the *a*-axis (α_a) and *c*-axis (α_c) were calculated based on the gradient of the linear fits obtained, which indicate anisotropic thermal expansion along the *c*-axis. For clarity, the lattice constants obtained at various temperatures were normalised relative to the initial lattice constants at room-temperature. **(e)** Layered structure of $Na_2Ni_2TeO_6$ explicitly showing the arrangement of Na atoms along with NiO_6 and TeO_6 octahedra along the *a*-axis and *c*-axis that can rationalize the results obtained in (d).

Another characteristic notable in the XRD patterns of $Na_2Ni_2TeO_6$, is that the Bragg peaks for instance, (002) and (100) shift towards lower diffraction angles with increase in temperature (**Figure 2c**), indicating thermal lattice expansion with temperature elevation. However, the reversibility of the changes was confirmed through comparison of the XRD patterns obtained before and after heating upon cooling down to room temperature (**Supplementary Figure 2**). It should be noted that expansion of the lattice constant that defines the dimension along the *c*-axis (*c*) is more conspicuous than that along the *a*-axis (*a*), as shown in **Figure 2d** and summarised in **Supplementary Table 1**. This anisotropic thermal expansion can be quantified by determining the respective coefficients of thermal expansion (α_c and α_a, respectively) through evaluating the gradient of the linear regression. α_c is found to be 2.7 times larger than α_a ($=1.00\times10^{-5}$ K^{-1}). This disparity in expansion is as a result of the magnitude difference between the inter- and intra-layer bonding in the honeycomb layered framework of $Na_2Ni_2TeO_6$. As the atoms within the honeycomb slab are bound by strong covalent Te–O and Ni–O bonds, expansion of the lattice along the *a*-axis (*a*-*b* plane) is severely restricted compared to the *c*-axis of the crystal which entails weaker Na–O bonds (as schematically illustrated in **Figure 2e**).

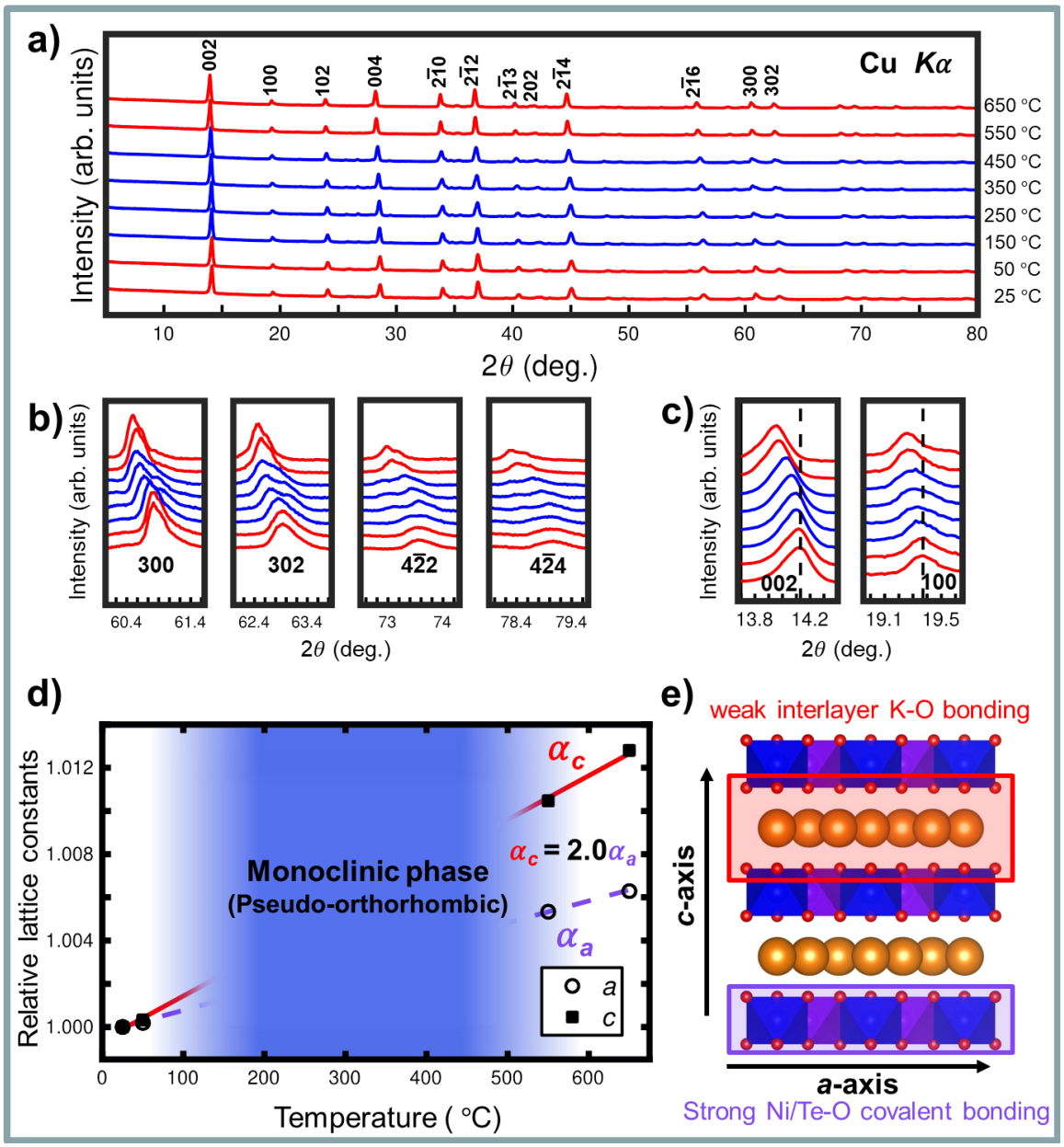

Figure 4. High-temperature XRD measurements of $K_2Ni_2TeO_6$. (a) Evolution of the XRD patterns of $K_2Ni_2TeO_6$ with increase in temperature from 25 °C to 650 °C. The room-temperature phase (indexed in a hexagonal lattice ($P6_3/mcm$ space group)) is shown in red, whilst a new intermediate monoclinic (pseudo-orthorhombic) phase is highlighted in blue. This intermediate phase further transforms back to the hexagonal lattice (red) with heating. **(b)** Appearance and extinction of Bragg diffraction peaks on heating, which attest to changes in the crystal symmetry. Notable is the appearance of (300), (302), (4-22) and (4-24) peaks of the monoclinic (pseudo-orthorhombic) phase that commences at around 130 °C. These peaks further merge at above 550 °C, hallmarking a reversion to the hexagonal lattice symmetry. **(c)** Shift of the (002) and

(100) Bragg peaks to lower diffraction angles with increase in temperature, indicating thermal lattice expansion along the *a*-axis and *c*-axis. **(d)** Quantification of the lattice expansion of the hexagonal lattice with increase in temperature by plotting the *a* and *c* lattice constants against the temperature to obtain the coefficients of thermal expansion (α_a and α_c). **(e)** Layered structure of $K_2Ni_2TeO_6$ explicitly showing the arrangement of K atoms along with NiO_6 and TeO_6 octahedra along the *a*-axis and *c*-axis that can rationalize the results obtained in (d).

In the case of $K_2Ni_2TeO_6$, two different phase transition regimes can be discerned from the XRD patterns taken between 25 °C and 650 °C, as shown in **Figure 4a**. Heating beyond 130 °C results in splitting of multiple peaks (**Figure 4b**) indicating a change in the lattice symmetry. This phase could be indexed to a monoclinic (pseudo-orthorhombic) lattice with the following lattice parameters: a = 4.526 Å, b = 5.250 Å, c = 12.446 Å, β =90.51° (at 150 °C). Further details are provided in **Supplementary Figure 3**. Even without the use of complementary neutron diffraction and transmission electron microscopy, which are beyond the scope of the present study, the occurrence of the phase transition inducing this intermediate phase can still be discerned. Further heating of this intermediate phase leads to the merging of the peaks, as shown in **Figure 4b**, finally reverting back to a hexagonal lattice indexed in the $P6_3/mcm$ space group. Moreover, akin to the trend observed in $Na_2Ni_2TeO_6$, Bragg peaks such as (002) and (100) shift towards lower diffraction angles with increase in temperatures (**Figure 4c**), indicating an overall thermal expansion of the $K_2Ni_2TeO_6$ lattice. As with $Na_2Ni_2TeO_6$, the weak interlayer bonds of $K_2Ni_2TeO_6$ lead to an anisotropic expansion of the *c*-axis with the α_c coefficient becoming 2.0 times larger than α_a (= 1.02×10^{-5} K^{-1}), as highlighted by **Supplementary Figure 4** and **Supplementary Table 2**). Upon cooling down, the XRD patterns of $K_2Ni_2TeO_6$ are a close match to those obtained before heating (**Supplementary Figure 5**), confirming the reversibility of the observed structural changes.

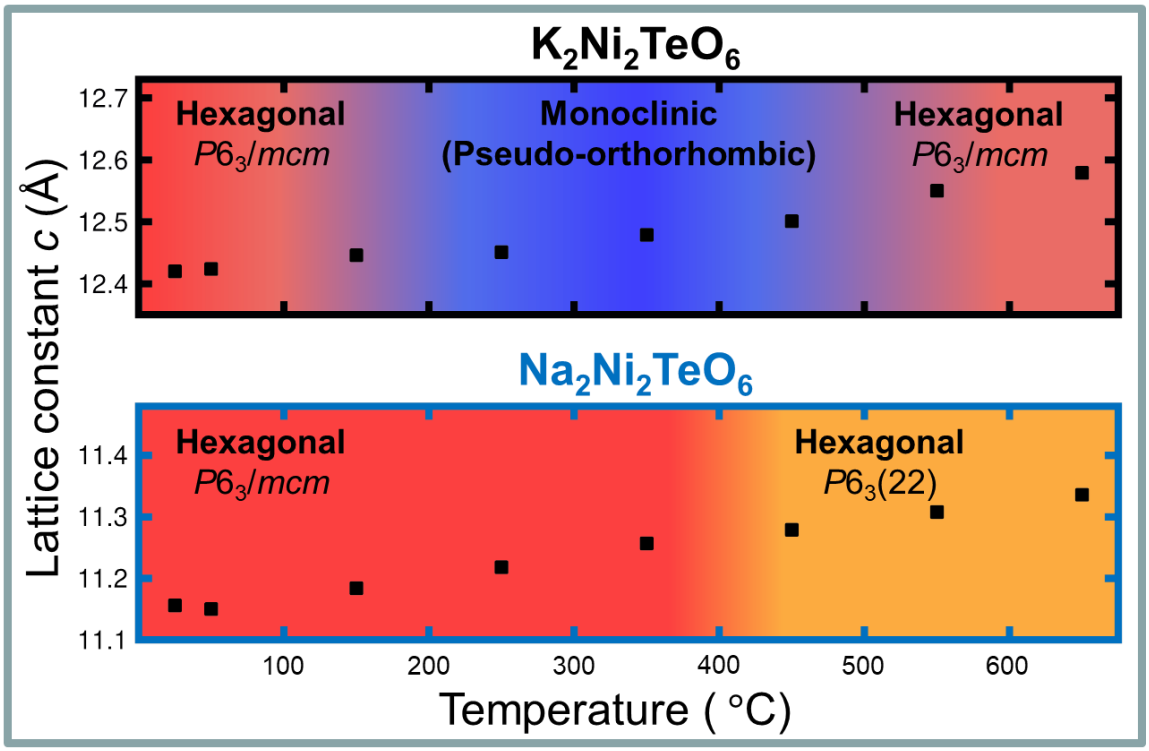

Figure 5. Phase transitions in $A_2Ni_2TeO_6$ (A = Na, K) induced by temperature. Changes in the lattice constants (c) along the c-axis with increase in temperature based on the analyses of the XRD patterns obtained. Phase transition regimes are illustrated using color variations for clarity.

Figure 5 provides a summary of the phase transitions observed in $A_2Ni_2TeO_6$ (A = Na, K) at high temperatures using XRD measurements. In $Na_2Ni_2TeO_6$, the phase transition entails a systematic expansion of the unit cell with increasing temperature, concomitant with a change in the symmetry of the hexagonal lattice (from a centrosymmetric $P6_3/mcm$ to a non-centrosymmetric $P6_3(22)$ space group). Although more comprehensive structural analyses could not be attained with conventional XRD measurements, a tentative structural model of the high-temperature $Na_2Ni_2TeO_6$ phase suggests that this phase transition involves a change in the manner of arrangement of the honeycomb slabs, as provided in **Supplementary Figure 6**. Pertaining to $K_2Ni_2TeO_6$, phase transition at high temperature entails a change from the hexagonal to a monoclinic (pseudo-orthorhombic) phase at intermediate temperatures, with reversion back to the hexagonal lattice upon further heating (as can be seen in **Supplementary Figure 5**).

The present results demonstrate that phase transitions in honeycomb layered oxides $A_2Ni_2TeO_6$ (A = Na, K) are not only electrochemically-induced,[12] but can also be induced through temperature elevation. Although, the mechanics of the phase transitions are yet to be extensively explored, multiple phase transitions attributed to the larger inter-slab distance are manifested in $K_2Ni_2TeO_6$. Neutron diffraction measurements complemented with electron microscopy may shed more light on the mechanics of phase transitions and their correlation with other attributes innate in this class of honeycomb layered oxide materials. More recently, Bera and co-worker attempted to unveil the variation of Na^+ dynamics in $Na_2Ni_2TeO_6$ with temperature,[28] albeit not at high temperatures enough to discern the phase transition revealed in this study. The central findings presented herein (*i.e.*, existence of temperature-induced phase transition in $Na_2Ni_2TeO_6$ and $K_2Ni_2TeO_6$) open new avenues for future exploration of phase transitions in related honeycomb layered oxides.

References

(1) Kanyolo, G. M.; Masese, T.; Matsubara, N.; Chen, C. –Y.; Rizell, J.; Forslund, O. K.; Nocerino, E.; Papadopoulos, K.; Zubayer, A.; Kato, M.; Tada, K.; Kubota, K.; Senoh, H.; Huang, Z. –D.; Sassa, Y.; Mansson, M.; Matsumoto, H.; Xu, Q. Honeycomb Layered Oxides: Structure, Energy Storage, Transport, Topology and Relevant Insights. arXiv 2020, arXiv:2003.03555.

(2) Schmidt, W.; Berthelot, R.; Sleight, A. W.; Subramanian, M. A. Solid Solution Studies of Layered Honeycomb-Ordered Phases O3-$Na_3M_2SbO_6$ (M = Cu, Mg, Ni, Zn). *J. Solid State Chem*. 2013, 201, 178–185.

(3) Yadav, D. K.; Sethi, A.; Shalu; Uma, S. New Series of Honeycomb Ordered Oxides, $Na_3M_2SbO_6$ (M(II) = Mn, Fe, (Mn, Fe), (Mn, Co)): Synthesis, Structure and Magnetic Properties. *Dalton Trans.* 2019, 48 (24), 8955–8965.

(4) Sankar, R.; Panneer Muthuselvam, I.; Shu, G. J.; Chen, W. T.; Karna, S. K.; Jayavel, R.; Chou, F. C. Crystal Growth and Magnetic Ordering of $Na_2Ni_2TeO_6$ with Honeycomb Layers and $Na_2Cu_2TeO_6$ with Cu Spin Dimers. *CrystEngComm*. 2014, 16 (47), 10791–10796.

(5) Karna, S. K.; Zhao, Y.; Sankar, R.; Avdeev, M.; Tseng, P. C.; Wang, C. W.; Shu, G. J.; Matan, K.; Guo, G. Y.; Chou, F. C. Sodium Layer Chiral Distribution and Spin Structure of $Na_2Ni_2TeO_6$ with a Ni Honeycomb Lattice. *Phys. Rev. B* 2017, 95 (10), 1–9.

(6) Kurbakov, A. I.; Korshunov, A. N.; Podchezertsev, S. Y.; Stratan, M. I.; Raganyan, G. V; Zvereva, E. A. Long-Range and Short-Range Ordering in 2D

Honeycomb-Lattice Magnet $Na_2Ni_2TeO_6$. *J. Alloys Compd.* 2020, 820, 153354.

(7) Zvereva, E. A.; Stratan, M. I.; Ovchenkov, Y. A.; Nalbandyan, V. B.; Lin, J. –Y.; Vavilova, E. L.; Iakovleva, M. F.; Abdel-Hafiez, M.; Silhanek, A. V; Chen, X. –J.; Stroppa, A.; Picozzi, S.; Jeschke, H. O.; Valenti, R.; Vasiliev, A. N. Zigzag Antiferromagnetic Quantum Ground State in Monoclinic Honeycomb Lattice Antimonates $A_3Ni_2SbO_6$ (*A* = Li,Na). *Phys. Rev. B* 2015, 92 (14), 144401.

(8) Zvereva, E. A.; Nalbandyan, V. B.; Evstigneeva, M. A.; Koo, H. –J.; Whangbo, M. –H.; Ushakov, A. V; Medvedev, B. S.; Medvedeva, L. I.; Gridina, N. A.; Yalovega, G. E.; Churikov, A. V; Vasiliev, A. N.; Büchner, B. Magnetic and Electrode Properties, Structure and Phase Relations of the Layered Triangular-Lattice Tellurate Li_4NiTeO_6. *J. Solid State Chem*. 2015, 225, 89–96.

(9) Derakhshan, S.; Cuthbert, H. L.; Greedan, J. E.; Rahaman, B.; Saha-Dasgupta, T. Electronic Structures and Low-Dimensional Magnetic Properties of the Ordered Rocksalt Oxides $Na_3Cu_2SbO_6$ and $Na_2Cu_2TeO_6$. *Phys. Rev. B* 2007, 76 (10), 104403.

(10) Viciu, L.; Huang, Q.; Morosan, E.; Zandbergen, H. W.; Greenbaum, N. I.; McQueen, T.; Cava, R. J. Structure and Basic Magnetic Properties of the Honeycomb Lattice Compounds $Na_2Co_2TeO_6$ and $Na_3Co_2SbO_6$. *J. Solid State Chem.* 2007, 180 (3), 1060–1067.

(11) Korshunov, A.; Safiulina, I.; Kurbakov, A. Spin Correlations and Short-Range Magnetic Order in the Honeycomb-Layered $Na_2Ni_2TeO_6$. *Phys. Status Solidi B* 2020, 257 (3), 1900232.

(12) Masese, T.; Yoshii, K.; Yamaguchi, Y.; Okumura, T.; Huang, Z. D.; Kato, M.; Kubota, K.; Furutani, J.; Orikasa, Y.; Senoh, H.; Sakaebe, H.; Shikano, M. Rechargeable Potassium-Ion Batteries with Honeycomb-Layered Tellurates as High Voltage Cathodes and Fast Potassium-Ion Conductors. *Nat. Commun.* 2018, 9 (1), 1–12.

(13) Masese, T.; Yoshii, K.; Kato, M.; Kubota, K.; Huang, Z. –D.; Senoh, H.; Shikano, M. A High Voltage Honeycomb Layered Cathode Framework for Rechargeable Potassium-Ion Battery: P2-Type $K_{2/3}Ni_{1/3}Co_{1/3}Te_{1/3}O_2$. *Chem. Commun*. 2019, 55 (7), 985–988.

(14) Yang, Z.; Jiang, Y.; Deng, L.; Wang, T.; Chen, S.; Huang, Y. A High-Voltage Honeycomb-Layered Na_4NiTeO_6 as Cathode Material for Na-Ion Batteries. *J. Power Sources* 2017, 360, 319–323.

(15) Yuan, D.; Liang, X.; Wu, L.; Cao, Y.; Ai, X.; Feng, J.; Yang, H. A Honeycomb-Layered $Na_3Ni_2SbO_6$: A High-Rate and Cycle-Stable Cathode for Sodium-Ion Batteries. *Adv. Mater.* 2014, 26 (36), 6301–6306.

(16) Sathiya, M.; Ramesha, K.; Rousse, G.; Foix, D.; Gonbeau, D.; Guruprakash,

K.; Prakash, A. S.; Doublet, M. L.; Tarascon, J. –M. Li_4NiTeO_6 as a Positive Electrode for Li-Ion Batteries. *Chem. Commun.* 2013, 49 (97), 11376–11378.

(17) Bhange, D. S.; Ali, G.; Kim, D. –H.; Anang, D. A.; Shin, T. J.; Kim, M. –G.; Kang, Y. –M.; Chung, K. Y.; Nam, K. –W. Honeycomb-Layer Structured $Na_3Ni_2BiO_6$ as a High Voltage and Long Life Cathode Material for Sodium-Ion Batteries. *J. Mater. Chem. A* 2017, 5 (3), 1300–1310.

(18) Yoshii, K.; Masese, T.; Kato, M.; Kubota, K.; Senoh, H.; Shikano, M. Sulfonylamide-Based Ionic Liquids for High-Voltage Potassium-Ion Batteries with Honeycomb Layered Cathode Oxides. *ChemElectroChem* 2019, 6 (15), 3901–3910.

(19) Wang, P. –F.; Weng, M.; Xiao, Y.; Hu, Z.; Li, Q.; Li, M.; Wang, Y. –D.; Chen, X.; Yang, X.; Wen, Y.; Yin, Y. –X.; Yu, X.; Xiao, Y.; Zheng, J.; Wan, L. –J.; Pan, F.; Guo, Y. –G. An Ordered Ni_6-Ring Superstructure Enables a Highly Stable Sodium Oxide Cathode. *Adv. Mater.* 2019, 31 (43), 1903483.

(20) Lu, X.; Xia, G.; Lemmon, J. P.; Yang, Z. Advanced Materials for Sodium-Beta Alumina Batteries: Status, Challenges and Perspectives. *J. Power Source*s 2010, 195 (9), 2431–2442.

(21) Evstigneeva, M. A.; Nalbandyan, V. B.; Petrenko, A. A.; Medvedev, B. S.; Kataev, A. A. A New Family of Fast Sodium Ion Conductors: $Na_2M_2TeO_6$ (*M* = Ni, Co, Zn, Mg). *Chem. Mater.* 2011, 23 (5), 1174–1181.

(22) Li, Y. ; Deng, Z; Peng, J. ; Gu, J. ; Chen, E. ; Yu, Y. ; Wu, J. ; Li, X. ; Luo, J. ; Huang, Y. ; Xu, Y. ; Gao, Z. ; Fang, C. ; Zhu, J. ; Li, Q. ; Han, J. ; Huang, Y. New P2-Type Honeycomb-Layered Sodium-Ion Conductor: $Na_2Mg_2TeO_6$. *ACS Appl. Mater. Interfaces* 2018, 10, 15760–15766.

(23) Wu, J. –F. ; Wang, Q. ; Guo, X. Sodium-ion conduction in $Na_2Zn_2TeO_6$ solid electrolytes. *J. Power Sources* 2018, 402, 513–518.

(24) Li, Y.; Deng, Z.; Peng, J.; Chen, E.; Yu, Y.; Li, X.; Luo, J.; Huang, Y.; Zhu, J.; Fang, C.; Li, Q.; Han, J.; Huang, Y. A P2-Type Layered Superionic Conductor Ga-Doped $Na_2Zn_2TeO_6$ for All-Solid-State Sodium-Ion Batteries. *Chem. – A Eur. J.* 2018, 24 (5), 1057–1061.

(25) Boyce, J. B.; Huberman, B. A. Superionic Conductors: Transitions, Structures, Dynamics. *Phys. Rep.* 1979, 51 (4), 189–265.

(26) Hull, S. Superionics: Crystal Structures and Conduction Processes. *Rep. Prog. Phys.* 2004, 67 (7), 1233–1314.

(27) Shannon, R. D. Revised Effective Ionic Radii and Systematic Studies of Interatomic Distances in Halides and Chalcogenides. *Acta Crystallogr. Sect. A* 1976, 32 (5), 751–767.

(28) Bera, A. K.; Yusuf, S. M. Temperature-Dependent Na-Ion Conduction and Its Pathways in the Crystal Structure of the Layered Battery Material $Na_2Ni_2TeO_6$. *J. Phys. Chem. C* 2020, 124 (8), 4421–4429.

Supplementary Information

Supplementary information will be availed online (access link to be appended during production).

Acknowledgements

We gratefully acknowledge Ms. Kumi Shiokawa, Mr. Masahiro Hirata and Ms. Machiko Kakiuchi for their advice and technical help as we conducted the syntheses, electrochemical and XRD measurements. This work was conducted in part under the auspices of the Japan Society for the Promotion of Science (JSPS KAKENHI Grant Number 19K15685), National Institute of Advanced Industrial Science and Technology (AIST) and Japan Prize Foundation.

Competing interests

The authors declare no competing interests.